Spin-density-wave effects on the elasticity of Cr - Ga alloy single crystals

1997 J. Phys.: Condens. Matter 9 9961

(http://iopscience.iop.org/0953-8984/9/45/024)

J. Phys.: Condens. Matter **9** (1997) 9961–9983. Printed in the UK PII: S0953-8984(97)85563-4

Spin-density-wave effects on the elasticity of Cr–Ga alloy single crystals

A R E Prinsloo, H L Alberts and P Smit

Department of Physics, Rand Afrikaans University, PO Box 524, Auckland Park 2006, Johannesburg, South Africa

Received 27 June 1997

Abstract. Measurements are reported of the temperature dependence of the elastic constants, ultrasonic attenuation and thermal expansion of dilute Cr–Ga alloy single crystals containing 0.16, 0.42 and 0.88 at.% Ga. Well defined magnetic anomalies were observed in all of these physical properties at the Néel temperature (T_N), at the incommensurate–commensurate (I–C) spin-density-wave (SDW) transition temperature (T_{IC}) and at the spin-flip transition temperature (T_{sf}). The complete magnetic phase diagram of the $Cr_{1-x}Ga_x$ alloy system has been determined for $x < 1$ at.% Ga from the temperatures of these anomalies. The magnetovolume ($\Delta\omega$) and the magnetic component (ΔB) to the bulk modulus were both found to vary as $a + bT^2 + cT^4$, as predicted by theory, in the ISDW phases of all three of the crystals. Values of the pressure derivatives of T_N for the crystals containing 0.16 at.% Ga and 0.42 at.% Ga were calculated from the results for ΔB and $\Delta\omega$. $dT_N/d\omega = (0.09 \pm 0.02) \times 10^5$ K calculated for the Cr + 0.16 at.% Ga crystal compares very well with the value $dT_N/d\omega = (0.108 \pm 0.006) \times 10^5$ K obtained from direct high-pressure measurements. High-pressure measurements have not been made on the Cr + 0.42 at.% Ga crystal for a comparison. The value $dT_{IC}/d\omega = (0.59 \pm 0.03) \times 10^5$ K calculated from $\Delta\omega$ and ΔB for Cr + 0.88 at.% Ga does not compare well with $dT_{IC}/d\omega = (0.17 \pm 0.07) \times 10^5$ K obtained from direct high-pressure measurements. This may point to inadequacies in the thermodynamic model used for the calculations. Predictions of microscopic theories for the temperature dependence of the ultrasonic attenuation, magnetovolume and the magnetic components of the elastic constants close to T_N do not fit the present measurements.

1. Introduction

The magnetic phase diagrams [1] of Cr alloys with group-3 nontransition metals Al and Ga contain a triple-point where the incommensurate (I) spin-density-wave (SDW) phase, the commensurate (C) SDW phase and the paramagnetic (P) phase coexist. The triple-point concentration (x_L) is around 2.2 at.% Al for the Cr–Al system and around 0.6 at.% Ga for the Cr–Ga system. The magnetoelasticity of polycrystalline Cr–Al and Cr–Ga alloys shows extraordinary effects [1]. It shows a singularity at a certain impurity concentration where the absolute values of certain of the magnetic Grüneisen parameters [1] reach unusually large peak values. For polycrystalline Cr–Al alloys the singularity occurs [1] at a concentration close to x_L, whereas it occurs at $x \approx 2x_L$ for polycrystalline Cr–Ga alloys. The last observation is unexpected as the singularity for Cr–Ga alloys is also expected [1] at $x \approx x_L$, where the Néel transition at T_N changes from an ISDW–P to a CSDW–P transition. Furthermore, the pressure derivative of the ISDW–CSDW phase transition temperature, T_{IC}, of Cr–Ga alloys is negative, in contrast with the case for all

0953-8984/97/459961+23$19.50

other Cr alloys studied up to now for which $dT_{IC}/dp > 0$. dT_{IC}/dp calculated from the magnetoelastic data for polycrystalline Cr–Ga alloys, using a thermodynamic model [1], is of opposite sign to that directly measured. For all other Cr alloy systems studied in the past, the signs of the directly measured dT_{IC}/dp agrees with that calculated from magnetoelastic data. dT_{IC}/dp has not yet been calculated from magnetoelastic data or measured directly for Cr–Al alloys for a comparison, as the ISDW–CSDW transition is not readily observed in the physical properties of this alloy system.

Magnetoelastic measurements on polycrystalline material are only of limited value and measurements of elastic constants on single-crystalline alloys are needed for a better understanding of the observed phenomena in Cr alloys with group-3 nontransition metals. Up to now the elastic tensor components c_{11}, c_{44} and $c' = \frac{1}{2}(c_{11} - c_{12})$ and their temperature dependences have only been studied experimentally [2–5] for single-crystalline Cr–Al alloys. These quantities for Cr–Al alloys show several interesting features. Both the longitudinal (c_{11}) and shear mode (c_{44} and c') elastic constants of Cr–Al alloys exhibit a well defined anomaly at the spin-flip transition temperature, T_{sf}, where the transverse ISDW state transforms to a longitudinal ISDW state on cooling. The Néel transition is characterized by deep minima in c_{11} for ISDW Cr–Al alloys ($x < x_L$) and by nearly steplike increases in c_{11} on increasing the temperature through T_N for CSDW Cr–Al alloy ($x > x_L$) single crystals [3]. For x not close to x_L the shear mode constant c' of Cr–Al alloys has a well defined anomaly at T_N, while the shear mode constant c_{44} shows only a weak anomaly, or for some Al concentrations none at all, at this temperature. A further interesting feature is that, for ISDW Cr–Al alloys ($x < x_L$), magnetic contributions to c_{11} persist up to $T \approx 3T_N$, whereas magnetic contributions to c' disappear abruptly at T_N. A Cr–Al alloy single crystal with x close to the triple-point concentration, $x_L \approx 2.2$ at.% Al, shows most interesting SDW effects in its elastic constants. For such an alloy the magnetic contributions to the bulk modulus, $B = \frac{1}{3}(c_{11} + 2c_{12})$, at low temperatures are [2] outstandingly large, being about 50% near 0 K. Furthermore, B for $x = 2.2$ at.% Al reaches [2] a shallow minimum at about 50 K after which it increases continuously, and linearly by about 50% on increasing the temperature up to 400 K. This means that a Cr–Al crystal with this critical composition becomes less compressible by about 50% as the temperature is increased from 50 K up to 400 K, in contrast with what is expected for normal metals. The SDW contributions to the shear constants c_{44} and c' of this critical-concentration Cr–Al alloy crystal, on the other hand, amount to less than 1% at 0 K and persist only up to about 100 K for c_{44} and to about 200 K for c'. Experiments [6] on polycrystalline Cr–Al alloys show that the polycrystalline shear constant, G, varies continuously through all of the magnetic phase transition temperatures without any trace of SDW effects, while the polycrystalline bulk modulus shows well defined anomalies of SDW origin at both T_{sf} and T_N. The ISDW–CSDW phase transition was not observed in the elastic constants of Cr–Al alloys, neither in those of polycrystalline nor single-crystalline alloys [3, 6].

The shear constant, G, of polycrystalline Cr–Ga alloys also varies [7] smoothly, without any anomaly, through all of the magnetic phase transition temperatures. Deep minima were however observed [7] in these alloys for B near T_N but T_{IC} was not well defined in B–T measurements [7]. No anomaly was observed in either B or G at the spin-flip transition temperature of polycrystalline Cr–Ga alloys. This is surprising as most Cr alloys show a magnetic anomaly in B at T_{sf} [1]. In order to get more insight into the complex magnetoelastic behaviour of Cr alloys with group-3 nontransition metals, we report here a study of the elastic constants, attenuation of ultrasonic waves and thermal expansion for three Cr–Ga alloy single crystals. Two of these crystals undergo ISDW–P

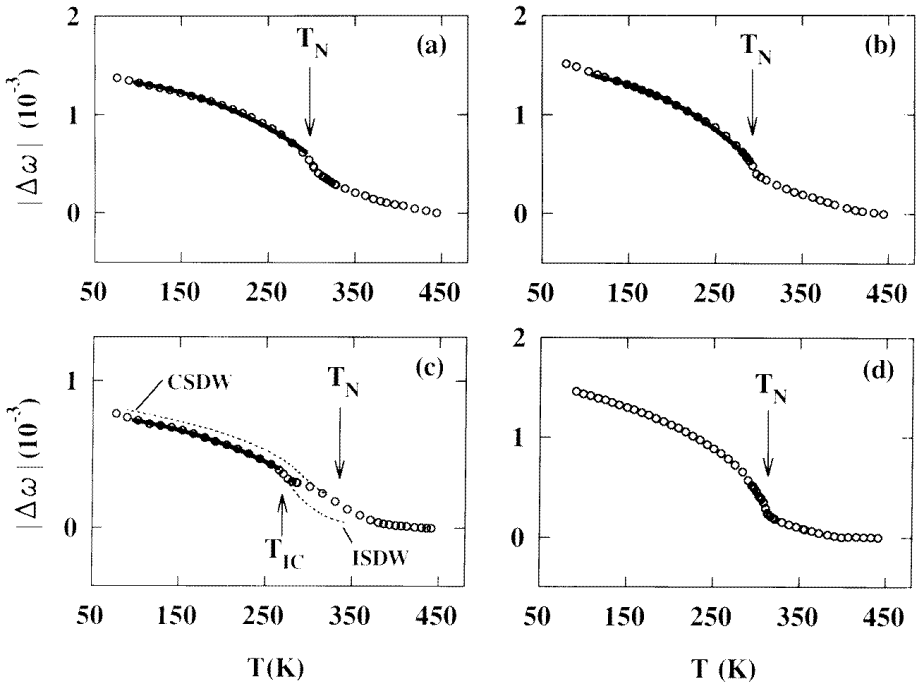

Figure 1. The absolute value, $|\Delta\omega|$, of the magnetovolume, $\Delta\omega$, as a function of temperature for single crystals of (a) Cr + 0.16 at.% Ga, (b) Cr + 0.42 at.% Ga, (c) Cr + 0.88 at.% Ga and (d) pure Cr. The solid curves are best fits of the equation $\Delta\omega = A_0 + A_1T^2 + A_2T^4$. The upper broken line, marked CSDW, in (c) represents the $|\Delta\omega|$–T curve expected if the crystal remains in the CSDW state from the paramagnetic state down to the lowest temperatures, without making a CSDW–ISDW phase transition. Similarly the lower broken line, marked ISDW, represents the $|\Delta\omega|$–T curve if the crystal remains in the ISDW phase at all temperatures below that of the paramagnetic state without making an ISDW–CSDW transition. The experimental points are marked: ○. Only a fraction of the measured points are shown for the sake of clarity.

phase transitions at T_N and the third, of which the composition is just above the triple-point concentration, undergoes both an ISDW–CSDW and a CSDW–P phase transition at T_{IC} and T_N, respectively.

2. Experimental methods

Three Cr–Ga alloy single crystals, containing 0.16, 0.42 and 0.88 at.% Ga, were grown by the floating-zone technique using RF heating in a pure argon atmosphere as previously described [8]. The starting materials were 99.996% pure Cr and 99.999% pure Ga. The actual concentrations of 0.16 ± 0.02 at.% Ga, 0.42 ± 0.03 at.% Ga and 0.88 ± 0.06 at.% Ga were determined using electron microprobe analysis techniques. The crystals were prepared with a pair of flat and parallel (110) faces and for some crystals also with flat and parallel (100) faces. The distance between these parallel faces was about 6 mm and the area of the flat surface about 30 mm^2. Standard ultrasonic techniques, phase comparison [9] and pulse–echo overlap [10] techniques, were used to measure the velocities for longitudinal or shear wave propagation along the [110] and [100] directions. 10 MHz quartz transducers

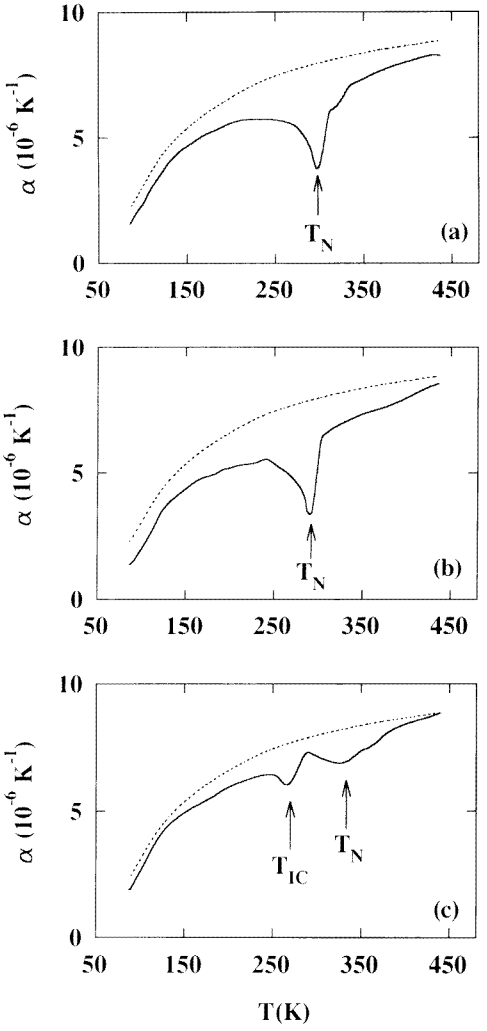

Figure 2. The coefficient of thermal expansion, α, as a function of temperature for (a) Cr + 0.16 at.% Ga, (b) Cr + 0.42 at.% Ga and (c) Cr + 0.88 at.% Ga. The broken lines show the temperature dependence of α for Cr + 5 at.% V [12], representing the nonmagnetic component of α for the Cr–Ga crystals.

were used for these measurements. The sensitivity of the former technique is 1 part in 10^3 or better and that of the latter about 1 part in 10^5. The error in the absolute values of the ultrasonic wave velocities is about 0.5 to 1%. The phase comparison method was more useful for measurements over a wide temperature range where the changes in ultrasonic wave velocity with temperature are large while the pulse–echo overlap technique was used for studies around the phase transition temperatures and for measuring ultrasonic wave attenuation near these temperatures. Measurements were made in the temperature range from 77 K to 450 K for the ultrasonic wave velocities while heating the sample slowly at a rate of about 0.5 K min^{-1}.

Thermal expansion measurements were made, as previously [8], by using a strain gauge technique. The measurements were done relative to Cr + 5 at.% V, which remains paramagnetic at all temperatures and serves to simulate [1, 6] the nonmagnetic component of the Cr–Ga crystals, i.e. $(\Delta L/L)_{meas} = (\Delta L/L)_{Cr_{95}V_5} - (\Delta L/L)_{Cr-Ga}$. The error in the absolute values of $\Delta L/L$ is about 5%, while changes of 3×10^{-7} with temperature could

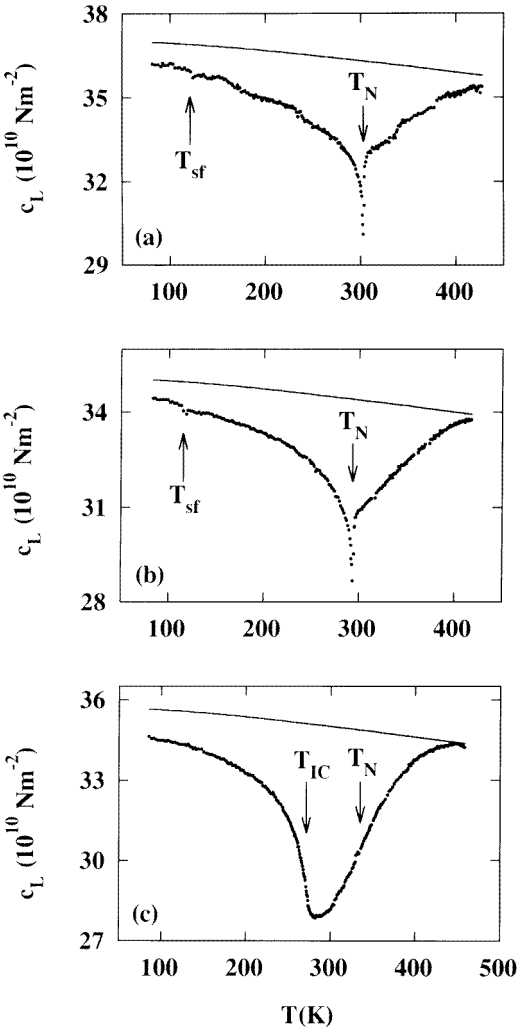

Figure 3. The temperature dependence (on heating) of the elastic constant $c_L = \frac{1}{2}(c_{11} + c_{12} + 2c_{44})$ for (a) Cr + 0.16 at.% Ga, (b) Cr + 0.42 at.% Ga and (c) Cr + 0.88 at.% Ga. The solid curves show the expected nonmagnetic behaviour determined using results on Cr + 5 at.% V [17].

be detected easily. Thermal expansion was measured along [100]. Measurements for the thermal expansion were recorded at 0.1 K intervals while slowly heating or cooling the samples at a rate of about 0.3 K min^{-1} in the temperature range 77 K to 450 K.

3. Results

3.1. Thermal expansion

As the crystals of this study are of cubic symmetry and as thermal expansion is represented by a tensor of the second rank, we do not expect [11] anisotropy in the thermal expansion for these alloys. The magnetovolume is directly given by $\Delta\omega = 3(\Delta L/L)_{meas}$. It is negative and its absolute value is shown as a function of temperature in figure 1. The results of Roberts *et al* [12] for the coefficient of thermal expansion, $\alpha_{Cr_{95}V_5}$, of Cr + 5 at.% V were used to calculate the coefficient of thermal expansion, α_{Cr-Ga}, of the Cr–Ga single crystals from $(\Delta L/L)_{meas}$. The results are shown in figure 2. Also shown in figure 2 is $\alpha_{Cr_{95}V_5}(T)$

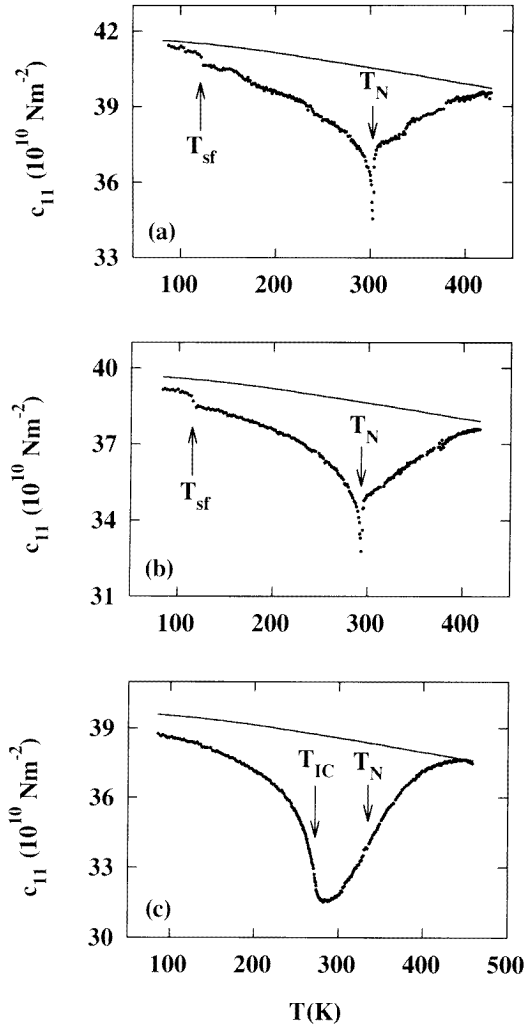

Figure 4. The temperature dependence of the elastic constant c_{11} for (a) Cr + 0.16 at.% Ga, (b) Cr + 0.42 at.% Ga and (c) Cr + 0.88 at.% Ga. The solid curves show the expected nonmagnetic behaviour determined using results on Cr + 5 at.% V [17].

which simulates [6] the nonmagnetic component of $\alpha_{\mathrm{Cr-Ga}}(T)$. $\alpha_{\mathrm{Cr-Ga}}(T)$ is shown as a smooth curve in figure 2. The scattering of the calculated $\alpha_{\mathrm{Cr-Ga}}$-values around this curve is to within 0.1×10^{-6} K^{-1}. Heating and cooling runs show no hysteresis effects in $(\Delta L/L)_{meas}$. For comparison the thermal expansion of a pure Cr single crystal was also measured. The results are shown in figure 1. No thermal hysteresis effects were observed during heating and cooling runs for pure Cr.

The $\Delta\omega$–T curves in figure 1 for pure Cr, Cr + 0.16 at.% Ga and Cr + 0.42 at.% Ga single crystals are very similar in shape. All three of these crystals remain in the ISDW phase at all $T < T_N$ with no I–C phase transition below T_N. The $\Delta\omega$–T curve for the Cr + 0.16 at.% Ga single crystal shows a more prominent 'kink' at T_N than that observed for a polycrystalline Cr–Ga alloy of the same concentration [7]. Also shown in figure 1(c) are two broken lines which represent what the $\Delta\omega$–T behaviour of Cr + 0.88 at.% Ga would be if it was to remain in either the ISDW or CSDW phase from $T = T_N$ down to $T = 0$ K, without any I–C transition. $|\Delta\omega|$ at 0 K as well as the Néel temperature is expected

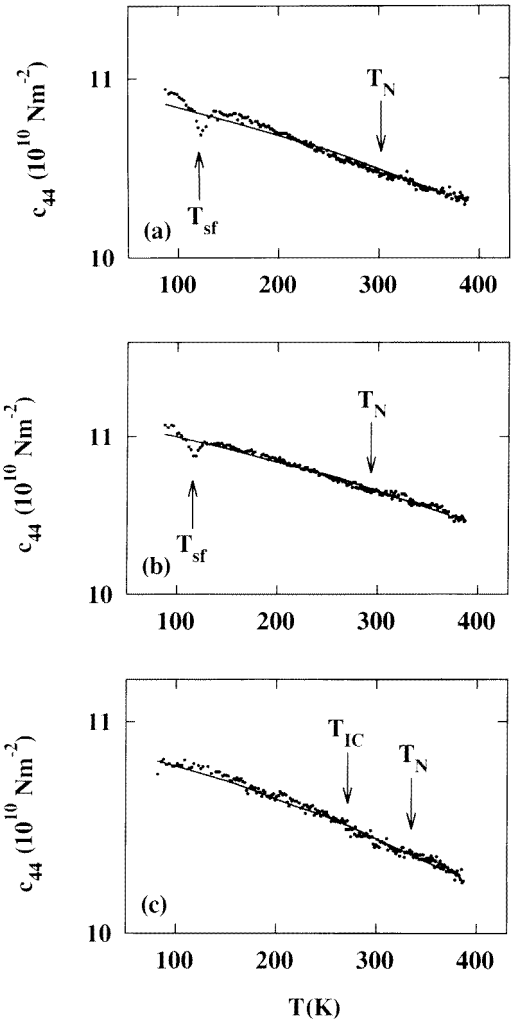

Figure 5. The temperature dependence of the elastic constant c_{44} for (a) Cr + 0.16 at.% Ga, (b) Cr + 0.42 at.% Ga and (c) Cr + 0.88 at.% Ga. The solid curves show the expected nonmagnetic behaviour determined using results on Cr + 5 at.% V [17].

[13] to be larger for a CSDW phase Cr–Ga alloy than for an ISDW phase one. This justifies the choice of the two different broken lines to represent the expected ISDW and CSDW curves for Cr + 0.88 at.% Ga in figure 1(c). For single-crystalline Cr + 0.88 at.% Ga the transition from the $\Delta\omega$–T broken curve, marked ISDW, to the $\Delta\omega$–T broken curve, marked CSDW, in figure 1(c), occurs at a sharp 'knee' point, followed by a smooth crossover in a more horizontal direction parallel to the T-axis. This gives rise to the low-temperature minimum in the α–T curve of figure 2(c). The temperature of this minimum was taken as the ISDW–CSDW phase transition temperature, T_{IC}, of the Cr + 0.88 at.% Ga crystal. Contrary to this, the crossover from the ISDW to CSDW phase at T_{IC} for polycrystalline Cr + 0.83 at.% Ga, in terms of figure 1(c), occurs by a smooth crossover in a more vertical direction parallel to the $|\Delta\omega|$-axis (figure 2(a) of reference [13]), resulting in a peak on the $|\Delta\omega|$–T curve and a maximum in α–T near T_{IC} [7]. There is a second minimum at $T > T_{IC}$ on the α–T curve (figure 2(c)) of single-crystalline Cr + 0.88 at.% Ga, similarly to what was observed [7] at T_N for polycrystalline Cr + 0.83 at.% Ga. We took T_N for the Cr + 0.88 at.% Ga single crystal at the temperature of this minimum (figure 2(c)). The

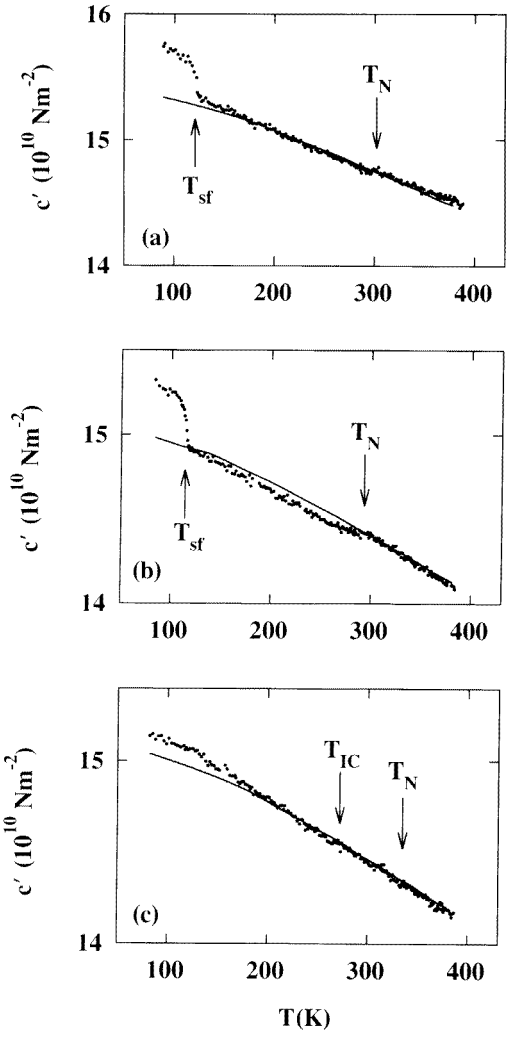

Figure 6. The temperature dependence of the elastic constant $c' = \frac{1}{2}(c_{11} - c_{12})$ for (a) Cr + 0.16 at.% Ga, (b) Cr + 0.42 at.% Ga and (c) Cr + 0.88 at.% Ga. The solid curves show the expected nonmagnetic behaviour determined using results on Cr + 5 at.% V [17].

reason that $\alpha(T)$ of the present Cr + 0.88 at.% Ga single crystal behaves differently during the I–C phase transition to that for the polycrystalline Cr + 0.83 at.% Ga alloy is currently unknown. The possibility of the existence of mixed ISDW/CSDW phases for temperatures in the transition region may partly be responsible for this. Evidence of such mixed states was previously found [8, 14] for instance for Cr–Si single crystals.

Both Cr + 0.16 at.% Ga and Cr + 0.42 at.% Ga crystals show a sharp minimum in the α–T curves of figure 2, similarly to the results obtained previously [7] for polycrystalline Cr–Ga alloys of similar concentrations. For Cr + 0.16 at.% Ga and Cr + 0.42 at.% Ga, T_N was defined at the minimum on the α–T curve for each as shown in figure 2. This gives $T_N = 298 \pm 2$ K for Cr + 0.16 at.% Ga and $T_N = 292 \pm 2$ K for Cr + 0.42 at.% Ga which correspond well with the values $T_N = 297$ K and $T_N = 290$ K obtained from measurements [7] on polycrystalline Cr + 0.15 at.% Ga and Cr + 0.42 at.% Ga alloys, respectively. For the Cr + 0.88 at.% Ga single crystal, $T_N = 335 \pm 10$ K and $T_{IC} = 270 \pm 5$ K from figure 2(c). These two values agree well with $T_N = 335$ K and $T_{IC} = 258$ K obtained [7] for

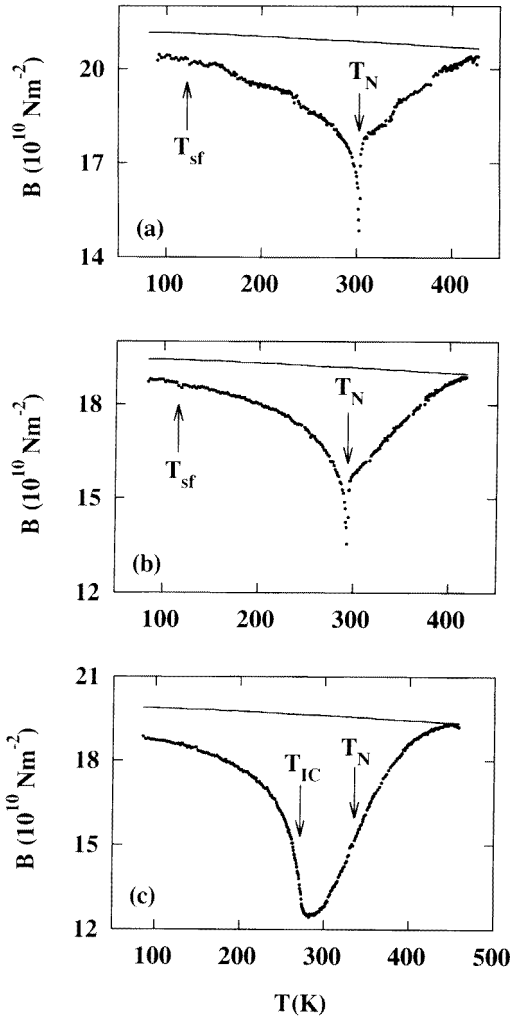

Figure 7. The temperature dependence of the bulk modulus $B = \frac{1}{3}(c_{11} + 2c_{12})$ for (a) Cr + 0.16 at.% Ga, (b) Cr + 0.42 at.% Ga and (c) Cr + 0.88 at.% Ga. The solid curves show the expected nonmagnetic behaviour determined using results on Cr + 5 at.% V [17]. T_{sf} shown in (a) and (b) was obtained from figure 5.

polycrystalline Cr + 0.83 at.% Ga.

As for most other Cr alloy systems thus far studied, the α–T curves of the Cr–Ga single crystals show very distinct minima at T_N. In the case of Cr–Al alloys with $x \ll x_L$, $\alpha(T)$ also shows [6] a minimum at T_N that becomes smaller [6] for x close to x_L, tends to disappear [2] at x_L and changes to a steplike anomaly at T_N for $x > x_L$ [6]. The Cr–Ga system differs from the Cr–Al system in this regard as it shows, for both of the present studies on a single crystal as well as previous [7] studies on polycrystalline alloys, a minimum at T_N for $x > x_L$ instead of a steplike increase with increasing temperature.

3.2. Elastic constants

The elastic constants were obtained from ultrasonic wave velocities and densities of the crystals by using standard equations [15] for cubic crystals. The densities were determined by hydrostatic weighing in water. Ultrasonic wave velocity data were corrected for transducer diffraction effects by using methods developed by Kittinger [16]. The elastic

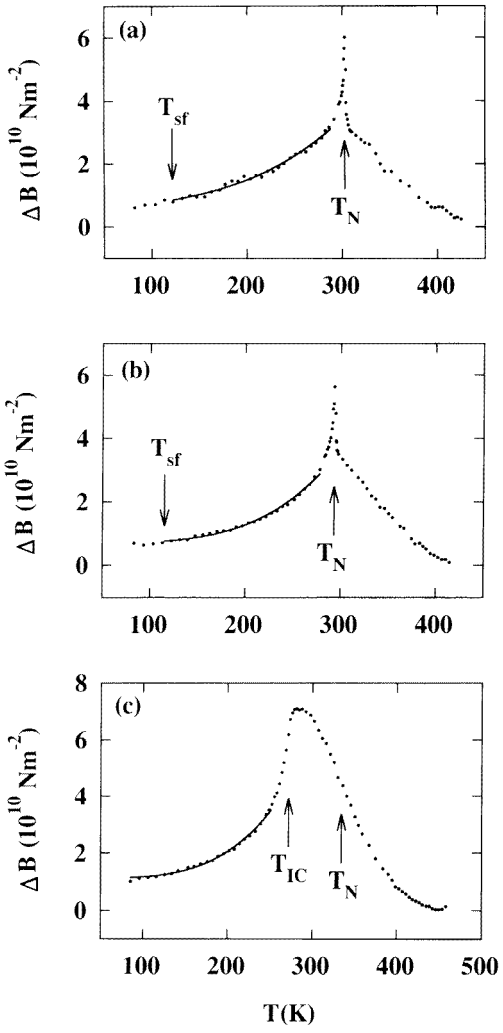

Figure 8. The temperature dependence of the magnetic contribution to the bulk modulus, $\Delta B = B_{\text{nonmagnetic}} - B_{\text{Cr–Ga}}$, for (a) Cr + 0.16 at.% Ga, (b) Cr + 0.42 at.% Ga and (c) Cr + 0.88 at.% Ga. The solid curves are best fits of the equation $\Delta B = B_0 + B_1T^2 + B_2T^4$. The values of T_{sf} shown are obtained from figure 5.

constants were corrected for the effects of thermal expansion of the sample by using the thermal expansion measurements reported in the previous section.

The temperature dependences of the elastic constants $c_L = \frac{1}{2}(c_{11} + c_{12} + 2c_{44})$, c_{11}, c_{44}, $c' = \frac{1}{2}(c_{11} - c_{12})$, and $B = \frac{1}{3}(c_{11} + 2c_{12})$ are shown, respectively, in figures 3, 4, 5, 6 and 7. $c_{11} = c_L + c' - c_{44}$ and the adiabatic bulk modulus $B = \frac{1}{3}(c_{11} + 2c_{12}) = c_L - c_{44} - \frac{1}{3}c'$ were calculated from the data obtained for c_L, c_{44} and c'. The solid lines in these figures represent the expected nonmagnetic behaviour and were obtained from the temperature dependences of the elastic constants [17] of a Cr + 5 at.% V crystal that remains paramagnetic at all temperatures down to 0 K. The magnetic contribution to the bulk modulus, $\Delta B = B_{\text{Cr}_{95}\text{V}_5} - B_{\text{Cr–Ga}}$, is obtained by subtracting the measured values of the Cr–Ga crystals from the broken curves in figure 7. Figure 8 shows the temperature dependence of ΔB.

The longitudinal mode elastic constants c_L and c_{11}, as well as B, show deep and sharp minima in figures 3, 4 and 7 for Cr + 0.16 at.% Ga and Cr + 0.42 at.% Ga. These two

crystals show I–P phase transitions at T_N and do not contain the CSDW phase in their magnetic phase diagrams. T_N for them was taken at the temperature of the deep minimum of the c_L–T curves of figures 3(a) and 3(b). This is similar to what was done previously [7] for polycrystalline Cr–Ga alloys with $x < x_L$. For Cr + 0.88 at.% Ga, for which $x > x_L$, c_L, c_{11} and B also show deep minima in figures 3, 4 and 7, but for this crystal the minima are very broad. The broadness of these minima may be ascribed to the closeness of T_{IC} and T_N in this crystal that is of a concentration just above the triple-point concentration. The inflection points to the left and to the right of the minimum in figures 3(c), 4(c) and 7(c) of Cr + 0.88 at.% Ga, agree very closely with T_{IC} and to T_N, respectively, obtained from the thermal expansion measurements of figure 2(c). In previous studies [7] on polycrystalline Cr + 0.83 at.% Ga the two inflection points at the broad minimum on the B–T curve were used to define T_{IC} and T_N. A similar definition seems to be appropriate for the present Cr + 0.88 at.% Ga crystal. Table 1 gives the transition temperatures obtained in this study from ultrasonic and thermal expansion measurements. The B–T minima observed for the Cr–Ga single crystals at T_N are very similar in shape to that observed for polycrystalline Cr–Ga alloys [7] with similar concentrations. The only difference is that the minimum for the Cr + 0.42 at.% Ga crystal is much narrower than that observed [7] for a Cr+ 0.42 at.% Ga polycrystalline alloy.

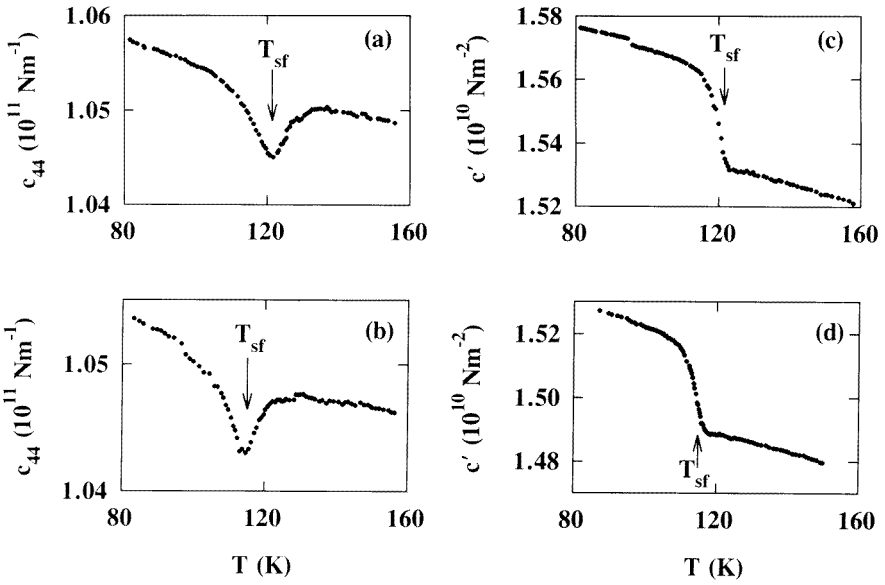

Figure 9. The temperature dependence of c_{44} near the spin-flip transition temperature, T_{sf}, of (a) Cr + 0.16 at.% Ga and (b) Cr + 0.42 at.% Ga. Also shown is the temperature dependence of c' near T_{sf} of (c) Cr + 0.16 at.% Ga and (d) Cr + 0.42 at.% Ga.

No magnetic anomalies were observed in the temperature range 77 K to 500 K for the shear modulus of polycrystalline Cr–Ga alloys [7]. For the Cr + 0.16 at.% Ga and Cr + 0.42 at.% Ga alloy single crystals, however, figures 5 and 6 depict small anomalies at T_N and very distinct anomalies at T_{sf} for the shear constants c_{44} and c'. The behaviour of c_{44} and c' for these two crystals close to T_{sf} is shown in figure 9. For the c_{44}-mode, T_{sf} was taken at the minimum of the curves shown in figures 9(a) and 9(b) for Cr + 0.16 at.% Ga and Cr + 0.42 at.% Ga, respectively. In the case of the c'-mode, T_{sf} was taken at the

Table 1. Magnetic transition temperatures T_{sf}, T_{IC} and T_N for Cr–Ga alloy single crystals obtained from thermal expansion, velocity of sound and ultrasonic (10 MHz) attenuation measurements.

(at.% Ga)	Transition temperature (K)	From thermal expansion	From ultrasonic velocity	From ultrasonic attenuation
0.16	T_{sf}	—	122 ± 2	120 ± 1
	T_N	298 ± 2	302.3 ± 0.9	303.1 ± 0.6
0.42	T_{sf}	—	115 ± 1	113.5 ± 0.5
	T_N	292 ± 2	292 ± 1	293.3 ± 0.3
0.88	T_{IC}	270 ± 5	272 ± 1	266 ± 6
	T_N	335 ± 10	328 ± 8	332 ± 2

inflection point at the sharp rise of the curves as shown in figures 9(c) and 9(d). Values of T_{sf} obtained from these two figures correspond well with each other and the average value for each alloy is shown in table 1.

It is of interest to compare the behaviour of the elastic constants of Cr–Ga and Cr–Al alloy single crystals as both of these two systems belong to the group of Cr alloy systems containing group-3 nontransition metals. First of all, the magnetic contributions to c_L, c_{11} and to B are considerably less at low temperatures in Cr–Ga than in Cr–Al crystals. For instance, for Cr–Al [4] at $x > x_L$, ΔB reaches values of 7×10^{10} N m^{-2} while it is only about 1×10^{10} N m^{-2} for the Cr + 0.88 at.% Ga crystal with $x > x_L$. Furthermore, a sharp anomaly is observed at T_{sf} on the B–T curve for a Cr–Al alloy single crystal with $x < x_L$ while it is negligibly small in figures 7(a) and 7(b) for Cr–Ga crystals with $x < x_L$. The absence of the B-anomaly in Cr–Ga may be ascribed to its smallness at T_{sf} for c_L, and to a near cancellation of the effects of the c_L-, c_{44}- and c'-anomalies in the equation $B = c_L - c_{44} - \frac{1}{3}c'$. Another difference between Cr–Ga and Cr–Al single crystals is the absence of any magnetic anomaly at T_{IC} in the elastic constants [4] and thermal expansion [6] of the latter, while both of these physical quantities show anomalies for the former at T_{IC}.

The ultrasonic attenuation coefficient, γ, for the c_{11}, c_{44}, c_L and c' propagation modes, γ_{11}, γ_{44}, γ_L and γ' respectively, near the transition temperatures for Cr + 0.16 at.% Ga, Cr + 0.42 at.% Ga and Cr + 0.88 at.% Ga are shown in figures 10, 11 and 12, respectively. The crystals used in this study were in the multi-$\boldsymbol{Q}$ SDW state since they were not field cooled through T_N. γ was also previously measured [18] for a Cr + 0.5 at.% V single crystal, for longitudinal sound propagation only, in both the multi-$\boldsymbol{Q}$ and single-$\boldsymbol{Q}$ states. For the multi-$\boldsymbol{Q}$ state this sample shows a small steplike decrease when the TISDW phase is entered with increasing temperature through T_{sf}. This is to be compared with the minima observed in γ_{11} and γ_L at T_{sf} for the Cr + 0.16 at.% Ga and Cr + 0.42 at.% Ga crystals in figures 10(a) and 10(b) and 11(a). Recently [19] γ was also studied near T_{sf} for Cr–Ir alloy single crystals in the multi-$\boldsymbol{Q}$ state containing 0.07 and 0.17 at.% Ir. For these crystals small peaks were observed at T_{sf} for γ_{11}, γ_{44} and γ'. This behaviour differs from that of the Cr + 0.16 at.% Ga crystal of the present study which shows minima for γ_{11}–T and γ_L–T at T_{sf} and more steplike decreases in γ'–T and γ_{44}–T. On the other hand, although γ_L–T for Cr + 0.42 at.% Ga also shows (figure 11) a minimum at T_{sf}, it does show a peak for γ'–T there, in line with the case of the Cr–Ir alloys. No anomaly was observed in γ_{44} for Cr + 0.42 at.% Ga at T_{sf}.

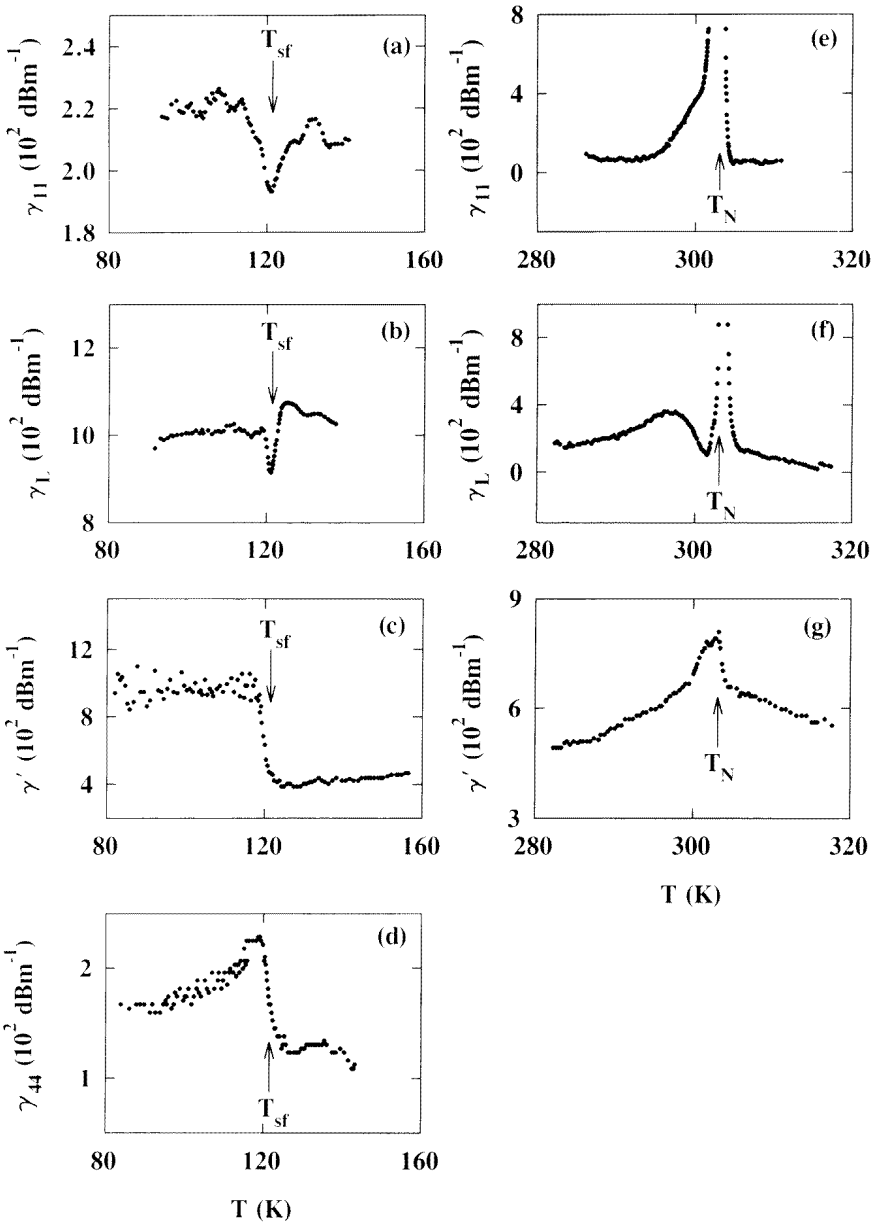

Figure 10. The temperature dependence of the ultrasonic (10 MHz) attenuation coefficients γ_{11}, γ_L, γ_{44} and γ', respectively for the c_{11}, c_L, c_{44} and c' wave propagation modes of Cr + 0.16 at.% Ga. Panels (a), (b), (c) and (d) show the behaviour near the spin-flip transition temperature, T_{sf}, and panels (e), (f) and (g) that near the Néel temperature, T_N. In panels (e) and (f), measurements could not be done above about 8×10^2 dB m^{-1} as this is the limit for the instrument used.

Figures 10(e), 10(f) and 10(g) show γ_{11}, γ_L and γ' as functions of temperature near T_N for the Cr + 0.16 at.% Ga crystal. No attenuation anomaly was observed at T_N for this crystal in the c_{44} propagation mode. Both of the longitudinal propagation modes

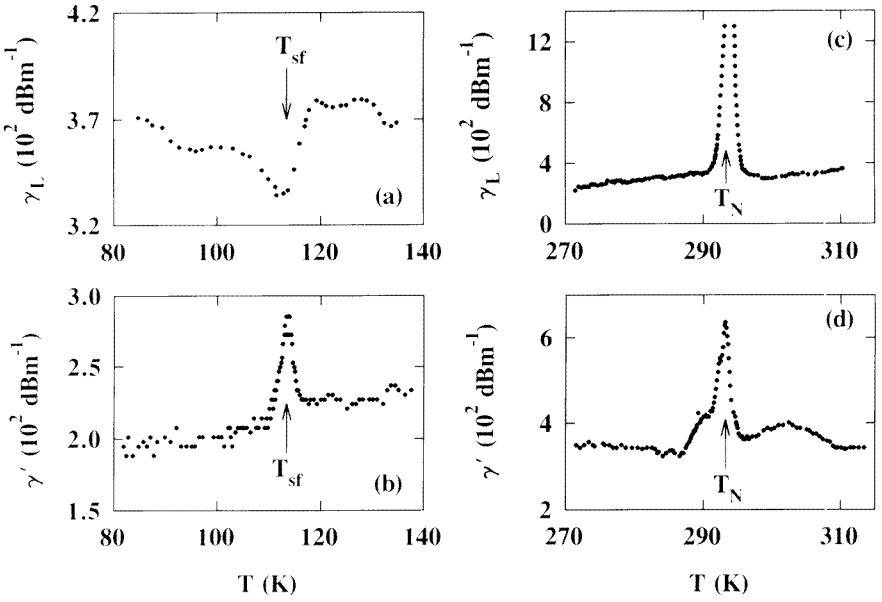

Figure 11. The temperature dependence of the ultrasonic (10 MHz) attenuation coefficients γ_L and γ', respectively, for the c_L and c' wave propagation modes of Cr + 0.42 at.% Ga. Panels (a) and (b) show the behaviour near the spin-flip transition temperature, T_{sf}, and panels (c) and (d) that near the Néel temperature, T_N. In panel (c) γ_L could not be measured above about 13 dB m^{-1} which is the limit for the equipment.

show a very large peak in the attenuation at T_N. There is also a peak in γ' at T_N for Cr + 0.16 at.% Ga, but it is not as sharp as that for γ_{11} and γ_L. In figures 10(e) and 10(f) the attenuation near T_N becomes extremely large, reaching values that are out of the range of our equipment. That is why we could not measure γ_{11} and γ_L for Cr + 0.16 at.% Ga in a temperature range of about 1 to 2 K around T_N in figures 10(e) and 10(f). This is also the case in figure 11(c) for Cr + 0.42 at.% Ga. Peaks also occur in γ_L–T and γ'–T at T_N for the Cr + 0.42 at.% Ga crystal as shown in figures 11(c) and 11(d). For the Cr + 0.88 at.% Ga crystal, a small broad peak, not too well defined, was observed near T_N for γ_L (figure 12(c)). The γ'–T curve of this crystal (figure 12(d)) shows a better defined peak, although fairly broad, near T_N. For Cr + 0.88 at.% Ga the peaks in γ_L–T and γ'–T near T_N are not as sharp and as prominent as those for Cr + 0.16 at.% Ga and Cr + 0.42 at.% Ga single crystals. Attenuation was also measured for γ_{44} for the Cr + 0.42 at.% Ga and Cr + 0.88 at.% Ga crystals but no magnetic anomalies were observed near T_N in this quantity for these two crystals. The values of T_N, defined at the temperatures of the peaks of the γ–T curves of the three Cr–Ga crystals, are given in table 1 and correspond well with values obtained from the thermal expansion and elastic constant measurements.

Figures 12(a) and 12(b) show γ_L–T and γ'–T curves for the Cr + 0.88 at.% Ga crystal near T_{IC}. Peaks are observed for these two quantities near T_{IC}, similarly to what was observed near T_{IC} for Cr–Ir [19] and Cr–Ru [20] single crystals. The values of T_{IC} taken at the midpoints of the peaks in figures 12(a) and 12(b) are given in table 1 and agree well with values obtained in the measurements of the thermal expansion and the velocity of sound. T_{IC} and T_N are completely resolved on the γ–T curves of figure 11 for Cr + 0.88 at.% Ga,

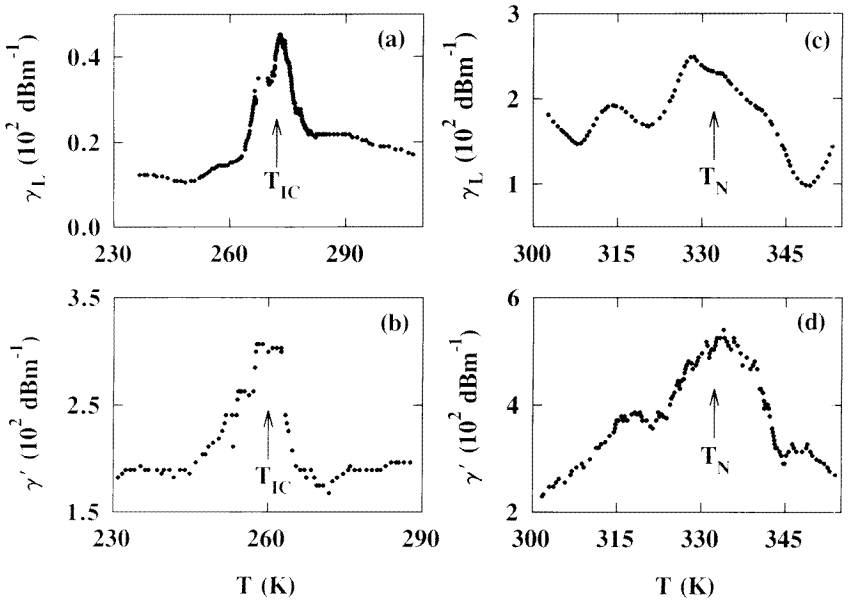

Figure 12. The temperature dependence of the ultrasonic (10 MHz) attenuation coefficients γ_L and γ', respectively for the c_L and c' wave propagation modes of Cr + 0.88 at.% Ga. Panels (a) and (b) show the behaviour near the ISDW–CSDW phase transition temperature, T_{IC}, and panels (c) and (d) that near the Néel transition, T_N. T_{IC} and T_N correspond to the values in figure 2.

as was also the case for the α–T curves of figure 2(c). These two transitions were however not that well resolved on the c_L–T and c_{11}–T curves of this crystal.

3.3. The magnetic phase diagram

The phase line separating the LISDW and TISDW phases in the magnetic phase diagram of the Cr–Ga alloy system has not been determined yet. The reason for this is that the LISDW–TISDW phase transition at T_{sf} does not show anomalies in physical properties like electrical resistivity, thermal expansion or elastic constants of polycrystalline Cr–Ga alloys. The present measurements on the single crystals, however, show well defined anomalies in the elastic constant at T_{sf}. The full magnetic phase diagram, constructed up to 1 at.% Ga from the data of table 1 and previous [7] measurements, is shown in figure 13.

The decrease in T_{sf} on alloying observed in figure 13 confirms the general trend for dilute Cr alloys and is explained [1] on the basis of the extra degree of freedom that is present if one has transverse rather than longitudinal polarization of the SDW.

4. Discussion

A thermodynamic model, previously successfully used for several Cr alloys [1, 8, 21–23], was used to analyse the magnetic contributions to the bulk modulus and the magnetovolume. The main assumptions of the model are that the magnetic free energy is separable from the total free energy and that volume strain terms in the free energy dominate shear strain effects. The last assumption is nearly fully satisfied for the present Cr–Ga alloy single

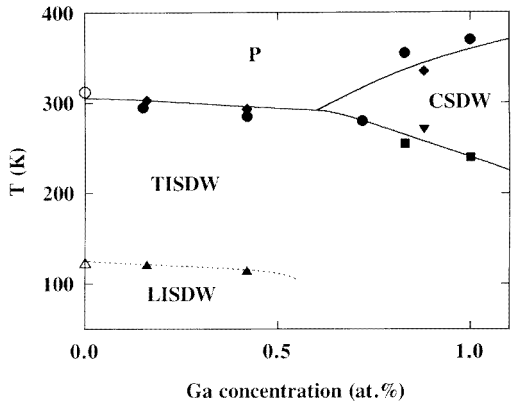

Figure 13. The magnetic phase diagram of Cr–Ga alloys. Points marked ▲ are for T_{sf} from this study as well as those marked ▼ for T_{IC} and ♦ for T_N. Points ● are for T_N and □ for T_{IC} from reference [7]. Points ○ and △ are for pure Cr [1].

crystals for which the magnetic contributions to B are very large compared to the very small, or near-zero, magnetic contributions to the shear elastic constants c_{44} and c' (figures 5, 6 and 7). The free energy in the thermodynamic model is given by

$$\Delta F(t,\omega) = \phi(\omega) f(t(\omega)) \tag{1}$$

where the excitation potential $\phi(\omega)$ depends on the volume strain, ω, in the low-temperature region well below T_N. $f(t(\omega))$ is taken [1] as $f(t(\omega)) = (1 - t^2)^2$ and the reduced temperature t is given by $t = T/T_0(\omega)$, with $T_0(\omega)$ a critical temperature parameter. It was found, to a good approximation, for Cr–Fe [23] and Cr–Si [8] alloys that T_0 is given by T_N. This approximation was also used in analysing the Cr–Ga data. It follows [8, 23] from equation (1) that

$$\Delta\omega = -(\partial\, \Delta F/\partial\omega)_T/B = a_0 + a_1 t^2 + a_2 t^4 \tag{2}$$

and

$$\Delta B = (\partial^2\, \Delta F/\partial\omega^2)_T = b_0 + b_1 t^2 + b_2 t^4 \tag{3}$$

where ΔB is the magnetic contribution to B, and $\Delta\omega$ is the magnetovolume.

From the theory it follows [23] that

$$\frac{a_1}{a_0} + \frac{a_2}{a_0} = -1 \tag{4}$$

$$\frac{\mathrm{d}\ln\phi}{\mathrm{d}\omega} = -\frac{8}{\Gamma_0}\left(\frac{\mathrm{d}\ln T_N}{\mathrm{d}\omega}\right)^2\left(\frac{b_1}{b_0} + \frac{b_2}{b_0} + 1\right)^{-1} = -4\left(\frac{a_1}{a_0} + 2\frac{a_2}{a_0}\right)^{-1}\left(\frac{\mathrm{d}\ln T_N}{\mathrm{d}\omega}\right) \tag{5}$$

and

$$\frac{\mathrm{d}\ln T_N}{\mathrm{d}\omega} = -\frac{\Gamma_0}{16}\left(5\frac{b_1}{b_0} + 3\frac{b_2}{b_0} + 7\right) \tag{6}$$

where

$$\Gamma_0 = b_0/Ba_0 = \Delta B(0)/B(0)\,\Delta\omega(0) \tag{7}$$

is the zero-temperature magnetic Grüneisen parameter.

Fawcett and Alberts [21, 22] considered ϕ in equation (1) to be constant for the temperature regions where $T \to T_N$ from above or from below. The above equations are therefore not valid in this limit. The following magnetic Grüneisen parameters are then obtained for these temperature regions:

$$\Gamma_{AF} = -\frac{\mathrm{d}\ln T_N}{\mathrm{d}\omega} = -\frac{1}{B_N T_N}\lim_{t\to 1}\left(\frac{\Delta B(t)}{\Delta\beta(t)}\right) \qquad t < 1 \tag{8a}$$

or

$$\frac{\mathrm{d}T_N}{\mathrm{d}\omega} = \frac{1}{B_N}\lim_{t\to 1}\left(\frac{\Delta B(t)}{\Delta\beta(t)}\right) \qquad t < 1 \tag{8b}$$

and

$$\Gamma_F = -\frac{\mathrm{d}\ln T_F}{\mathrm{d}\omega} = -\frac{1}{B_F T_F}\lim_{t\to 1}\left(\frac{\Delta B(t)}{\Delta\beta(t)}\right) \qquad t > 1 \tag{9a}$$

or

$$\frac{\mathrm{d}T_F}{\mathrm{d}\omega} = \frac{1}{B_F}\lim_{t\to 1}\left(\frac{\Delta B(t)}{\Delta\beta(t)}\right) \qquad t > 1. \tag{9b}$$

Here T_F is a characteristic spin-fluctuation temperature and $\Delta\beta = 3\,\Delta\alpha$ is the magnetic contribution to the coefficient of volume thermal expansion. The requirement that $\mathrm{d}T_N/\mathrm{d}\omega$ and $\mathrm{d}T_F/\mathrm{d}\omega$ be determined only in the limit $T \to T_N$ is not stringent [22]. For several Cr alloy systems the plots of $\Delta B(t)$ against $\Delta\beta(t)$ were found to be linear over a relatively wide temperature range above and below T_N [1, 8, 19, 23]. These linear parts are used to calculate $\mathrm{d}T_N/\mathrm{d}\omega$ and $\mathrm{d}T_F/\mathrm{d}\omega$ from equations (8) and (9). Values of B_N or B_F are calculated using

$$B_N \text{ or } B_F = \left\langle \sum_{t=t_0}^{t_i}\left[B_{\mathrm{Cr-Ga}}(t) + \frac{1}{2}\,\Delta B(t)\right]\right\rangle \tag{10}$$

where t_0 and t_i represent the beginning and the end of the temperature interval for $t < 1$ or $t > 1$ over which the ΔB–$\Delta\beta$ curves are linear.

Table 2. Coefficients in the expansions $\Delta\omega = a_0 + a_1t^2 + a_2t^4$, for the magnetovolume, and $\Delta B = b_0 + b_1t^2 + b_2t^4$, for the magnetic contribution to the bulk modulus, B, in the ISDW phases of the Cr–Ga alloy single crystals. Also given are values for $(a_1 + a_2)/a_0$.

	$\Delta\omega = a_0 + a_1t^2 + a_2t^4$			$\Delta B = b_0 + b_1t^2 + b_2t^4$			
(at.% Ga)	a_0 (10^{-3})	a_1 (10^{-3})	a_2 (10^{-3})	b_1 (10^9 N m^{-2})	b_0 (10^9 N m^{-2})	b_2 (10^9 N m^{-2})	$a_1/a_0 + a_2/a_0$
0.16	1.397 ±0.003	−0.64 ±0.01	−0.20 ±0.01	6.0 ±0.3	14 ±1	15 ±2	−0.60 ±0.02
0.42	1.493 ±0.003	−0.63 ±0.01	−0.34 ±0.01	7.1 ±0.2	−1 ±1	27 ±1	−0.646 ±0.008
0.88	0.776 ±0.001	−0.432 ±0.004	−0.074 ±0.006	11.3 ±0.3	−2 ±2	64 ±3	−0.65 ±0.01

Equations (2) and (3) fit the experimental results well over a wide temperature range of about 160 K, or more, below T_N for the ISDW phases of the three Cr–Ga alloy single crystals. The fitting parameters obtained are given in table 2. The fitting parameters are of the same order of magnitude as those previously obtained for Cr–Fe [23] and Cr–Si [8]. The fitted curves are shown as solid lines in figures 1 and 8. The solid lines shown in these figures are the best fits of the equations $\Delta B(T) = B_0 + B_1T^2 + B_2T^4$ and $\Delta\omega(T) = A_0 + A_1T^2 + A_2T^4$, from which ($a_0$, a_1, a_2) and (b_0, b_1, b_2) can be obtained. For the Cr + 0.88 at.% Ga crystal the fit was done in the ISDW phase below T_{IC}. This means that T_N used in the reduced temperature $t = T/T_N$ of the theory, when applied to this crystal, should be T_N for the Cr + 0.88 at.% Ga crystal if it was to remain in the ISDW

Table 3. Néel temperatures, T_N, the magnetovolume at 0 K, $\Delta\omega(0)$, the magnetic contribution to the bulk modulus at 0 K, $\Delta B(0)$, the bulk modulus at 0 K, Γ_0, $\mathrm{d}\ln T_N/\mathrm{d}\omega$, $\mathrm{d}\ln\phi/\mathrm{d}\omega$ and $\mathrm{d}T_N/\mathrm{d}\omega$ for Cr alloy single crystals. The value of $\mathrm{d}\ln\phi/\mathrm{d}\omega$ in brackets were calculated from (a_0, a_1, a_2) and those not in brackets from (b_0, b_1, b_2) using equation (5). The value $T_N = 300$ K for Cr + 0.88 at.% Ga was estimated for this crystal if it remains in the ISDW phase from 0 K up to the Néel point (figure 1(c)). The value $\mathrm{d}T_N/\mathrm{d}\omega$ in the table for this crystal is for this ISDW phase.

(at.% Ga)	T_N (K)	$\Delta\omega(0)$ (10^{-3})	$\Delta B(0)$ (10^9 N m^{-2})	$B(0)$ (10^{11} N m^{-2})	Γ_0	$\mathrm{d}\ln T_N/\mathrm{d}\omega$	$\mathrm{d}\ln\phi/\mathrm{d}\omega$	$\mathrm{d}\ln T_N/\mathrm{d}\omega$ (10^5)
0.16	303 ±1	1.418 ±0.007	6.0 ±0.3	2.09 ±0.02	−20 ±1	32.9 ±0.3	70 ±20 (180) (±20)	0.100 ±0.009
0.42	293.2 ±1	1.61 ±0.03	7.1 ±0.2	1.914 ±0.007	−23 ±1	26 ±2	50 ±20 (120) (±10)	0.076 ±0.006
0.88	300	0.77 ±0.01	11.3 ±0.3	1.94 ±0.01	−75 ±3	118 ±8	200 ±60 (630) (±40)	0.35

phase at all $T < T_N$, without an ISDW–CSDW phase transition. This T_N is not known but it should be lower than the experimental T_N for the CSDW–P transition at 335 K of this crystal, as shown by the rough extrapolation of the ISDW broken line in figure 1(c). A rough estimation for T_N of the ISDW phase is $T_N(\mathrm{ISDW}) \approx 300$ K from the ISDW broken line in figure 1(c). The fitting parameters shown in table 2 for this crystal were obtained using $T_N(\mathrm{ISDW}) = 300$ K. The experimental errors shown for the fitting parameters of Cr + 0.88 at.% Ga in table 2 are only that of the fit and do not include the error in the estimated $T_N(\mathrm{ISDW})$. For Cr + 0.42 at.% Ga and Cr + 0.88 at.% Ga the coefficient b_1 in ΔB is relatively small. The major contribution to the temperature dependence of ΔB in the ISDW phases of these two crystals comes from the t^4-term. This was also the case for Cr–Si alloys [8] but not for Cr–Fe [23] alloys. The left-hand side of equation (4) was calculated from the results of the fits, and the results are shown in table 2. The values of $(a_1 + a_2)/a_0$ are similar to those obtained in previous studies for Cr–Si [8], Cr–Fe [23] and Cr–Ir [19] and are in reasonable agreement with the theoretical value −1, if the approximations of the thermodynamic model are kept in mind. Tabulated in table 3 are the values calculated for Γ_0, $\mathrm{d}\ln\phi/\mathrm{d}\omega$, $\mathrm{d}\ln T_N/\mathrm{d}\omega$ and $\mathrm{d}T_N/\mathrm{d}\omega$, using equations (5), (6) and (7). $\mathrm{d}T_N(\mathrm{ISDW})/\mathrm{d}\omega$ is given for Cr + 0.88 at.% Ga. Also shown in table 3 are the values of T_N, $\Delta B(0)$, $\Delta\omega(0)$ and $B(0)$ used in these calculations. The values of T_N used in these calculations were determined from the minima of the v_L–T curves for Cr + 0.16 at.% Ga and Cr + 0.42 at.% Ga. Values of $\mathrm{d}\ln\phi/\mathrm{d}\omega$ calculated separately from (a_0, a_1, a_2) or (b_0, b_1, b_2), differ by a factor of up to about three (table 3), as was also found for Cr–Fe [23] and Cr–Si [8]. The reason for the discrepancy is currently unknown but it may partly be attributed to the approximations in the thermodynamic model.

Plots of ΔB against $\Delta\beta$ at each temperature are shown in figure 14. The curves were found to be reasonably linear over a relative large temperature range above and below T_N for both Cr + 0.16 at.% Ga and Cr + 0.42 at.% Ga which remain in the ISDW phase for

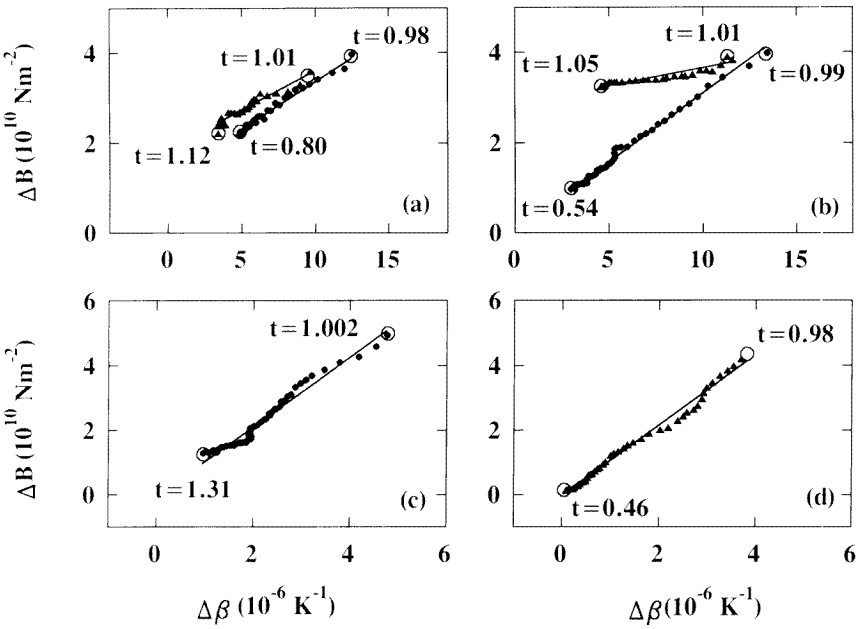

Figure 14. The magnetic contribution to the bulk modulus, ΔB, as a function of the magnetic contribution to the volume thermal expansion coefficient, $\Delta\beta$, at the same temperature for (a) Cr + 0.16 at.% Ga, (b) Cr + 0.42 at.% Ga and (c) and (d) Cr + 0.88 at.% Ga. In panels (a) and (b) points marked ▲ are for $t = T/T_N > 1$ and points marked ● are for $t < 1$. Panel (c) is for Cr + 0.88 at.% Ga at $t = T/T_N > 1$ and panel (d) is for the same crystal at $t = T/T_{IC} < 1$. For clarity, data are only shown in the linear regions of the plots, and for further clarity, only a fraction of the data points are shown. The solid curves are least-squares fits to the data and values of t at the encircled points are given in each panel.

Table 4. Values of T_N, $\Delta B(t)/\Delta\beta(t)$ determined from figure 14 and B_N, B_F or B_{IC} for the Cr–Ga alloy single crystals. Also given are values of $dT_N/d\omega$, $dT_{IC}/d\omega$ and $dT_F/d\omega$ calculated using equations (8), (9) and (11). For Cr + 0.88 at.% Ga, $\Delta B(t)/\Delta\beta(t)$ are given for $t = T/T_N > 1$ and for $t = T/T_{IC} < 1$.

		$\Delta B(t)/\Delta\beta(t)$ (10^{15} N m^{-2} K)		B_N, B_F or B_{IC} (10^{11} N m^{-2})				
(at.% Ga)	T_N (K)	$t < 1$	$t > 1$	$t < 1$	$t > 1$	$dT_N/d\omega$ (10^5 K)	$dT_{IC}/d\omega$ (10^5 K)	$dT_F/d\omega$ (10^5 K)
0.16	303 ±1	2.10 ±0.04	1.75 ±0.06	1.95 ±0.08	1.95 ±0.08	0.108 ±0.006	—	0.090 ±0.006
0.42	293 ±1	3.03 ±0.02	0.79 ±0.06	1.83 ±0.07	1.74 ±0.07	0.165 ±0.008	—	0.045 ±0.005
0.88	335 ±5	10.8 ±0.1	10.91 ±0.08	1.85 ±0.07	1.87 ±0.08	—	0.59 ±0.03	0.58 ±0.03

$T < T_N$. The Cr + 0.88 at.% Ga single crystal, which lies just above the triple-point concentration, contains a CSDW phase for $T_{IC} < T < T_N$ and we could not find useful linear regions of ΔB against $\Delta\beta$ for the CSDW phase. The linear regions shown in figures 14(c) and 14(d) are for $T > T_N$ and $T < T_{IC}$, respectively. The slopes obtained from these

curves are tabulated in table 4 together with values calculated for $dT_N/d\omega$ and $dT_F/d\omega$ using equations (8) and (9) for Cr + 0.16 at.% Ga and Cr + 0.42 at.% Ga.

An equation similar to equation (8) holds [21] for the ISDW–CSDW transition at T_{IC}, that is,

$$\frac{dT_{IC}}{d\omega} = \frac{1}{B_{IC}} \lim_{t\to 1}\left(\frac{\Delta B(t)}{\Delta\beta(t)}\right) \tag{11}$$

where B_{IC} is the value of B defined similarly to equation (10) for $T < T_{IC}$. From the slopes of figures 14(c), at $T > T_N$, and 14(d), at $T < T_{IC}$, $dT_F/d\omega$ and $dT_{IC}/d\omega$ can thus be calculated for Cr + 0.88 at.% Ga using, respectively, equations (9) and (11). These values are also shown in table 4.

For most dilute Cr alloys previously studied, it was found that $dT_N/d\omega < dT_F/d\omega$ [8, 19]. This means that the short-range magnetic order and spin fluctuations above T_N are more volume dependent than the SDW below T_N. From table 4 the situation is however just the reverse for Cr + 0.16 at.% Ga and Cr + 0.42 at.% Ga; $dT_N/d\omega > dT_F/d\omega$. This phenomenon was recently also observed for a Cr + 0.17 at.% Ir single crystal [19]. The reason for the unusual behaviour of the Cr–Ga samples is currently not known. For the Cr + 0.88 at.% Ga crystal it is interesting to note that $dT_F/d\omega$ is more than six times larger than that for the other two Cr–Ga crystals. As the latter two crystals have ISDW–P transitions at T_N and the former one a CSDW–P transition, it is tempting to conclude that spin fluctuations at temperatures above a CSDW–P transition in Cr–Ga alloys are more volume dependent than those above an ISDW–P transition.

The values of $dT_N/d\omega$ and $dT_{IC}/d\omega$ of table 4, calculated using the thermodynamic model, are to be compared with values obtained from direct high-pressure measurements. High-pressure measurements were performed on the Cr + 0.16 at.% Ga and Cr + 0.88 at.% Ga crystals. Figure 15(a) shows the longitudinal wave velocity, v_L, along [110], as a function of temperature for different constant pressures for Cr + 0.16 at.% Ga. The Néel point at each pressure was taken at the minimum on the v_L–T curve. The pressure dependence of T_N is shown in figure 15(b). T_N varies linear with pressure giving $dT_N/dp = -(64 \pm 4)$ K GPa^{-1}. $dT_N/d\omega$ was calculated from dT_N/dp using [24]

$$\frac{d\ln T_N}{d\omega} = -B\frac{dT_N}{dp}\left(1 - 3\alpha B\frac{dT_N}{dp}\right)^{-1}. \tag{12}$$

From equation (12) a value $dT_N/d\omega = (0.09 \pm 0.02) \times 10^5$ K is obtained which compares reasonably well with the value $dT_N/d\omega = (0.108 \pm 0.006) \times 10^5$ K obtained from an application of the thermodynamic model to the magnetoelastic measurements (table 4). Direct high-pressure measurements were not performed for the Cr + 0.42 at.% Ga crystal. Our high-pressure measurements on the Cr + 0.88 at.% Ga crystal were reported previously [25]. In that study we obtained $dT_{IC}/dp = -(174 \pm 29)$ K GPa^{-1} for this crystal. Using this value in equation (12) gives $dT_{IC}/d\omega = (0.17 \pm 0.07) \times 10^5$ K compared to a value $dT_{IC}/d\omega = (0.59 \pm 0.03) \times 10^5$ K (table 4) obtained from the magnetoelastic data. The reason for the large discrepancy between these two values of $dT_{IC}/d\omega$ is currently unknown and may partly be due to inadequacies of the thermodynamic model. What is however of importance is that the signs of $dT_{IC}/d\omega$ obtained using the two different methods agree: they are both positive, for single-crystalline Cr + 0.88 at.% Ga. In the case of polycrystalline Cr–Ga alloys, however, the directly measured $dT_{IC}/d\omega$ (positive) differs in sign (negative) with that obtained from magnetoelastic measurements, using the thermodynamic model [1]. We do not know currently why polycrystalline and single-crystalline Cr–Ga alloys differ in this regard.

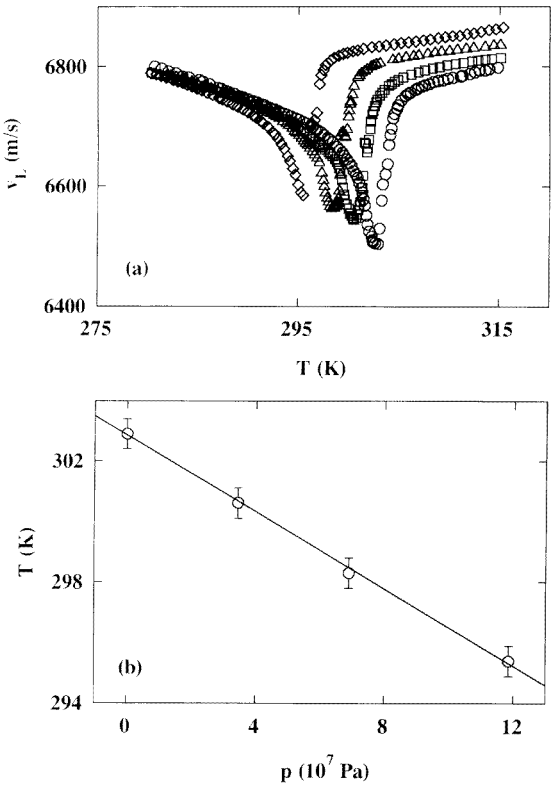

Figure 15. (a) The ultrasonic wave velocity, v_L, for the c_L wave propagation mode of Cr + 0.16 at.% Ga as a function of temperature at different constant pressures: ○, 0 GPa; □, 0.04 GPa; △, 0.07 GPa; and ◇, 0.12 GPa. (b) The pressure dependence of the Néel temperature of Cr + 0.16 at.% Ga.

Table 5. Values of the slope, m, obtained from the least-squares fits to the linear regions of plots of $\log\gamma$ against $\log|(1 - T/T_N)|$ for Cr + 0.16 at.% Ga and Cr + 0.42 at.% Ga. These plots were made after subtracting the background attenuation from the measured attenuation coefficient, γ. The temperature range in which the plots are linear is given by the difference between the temperatures T_{begin} and T_{end}.

			$T > T_N$			$T > T_N$		
(at.% Ga)	Mode	T_N (K)	m	T_{begin} (K)	T_{end} (K)	m	T_{begin} (K)	T_{end} (K)
0.16	c_{11}	302.6 ±0.6	−7.0 ±0.2	303.8	304.3	−0.76 ±0.02	298.7	301.6
0.42	c_L	293.7 ±0.7	−2.53 ±0.06	294.5	298.0	—	—	—

Sato and Maki [26] studied the ultrasonic attenuation of dilute Cr alloys above T_N theoretically. They found that for both longitudinal and shear waves γ should diverge as $(T/T_N - 1)^{-1/2}$ for a transition from the paramagnetic state into the ISDW state. No divergence is expected for a transition into the CSDW state. For concentrations in the

vicinity of the triple-point concentration, a divergence as $(T/T_N - 1)^{-5/4}$ is expected. We attempted to test Sato and Maki's theory for the present Cr–Ga alloy single crystals. A problem is however the determination of the background attenuation below and above T_N in figures 10, 11 and 12. The background could be determined meaningfully for only three cases: for the γ_{11}–T curve (figure 10(e)), both for $T > T_N$ and $T < T_N$, for the γ_L–T curve (figure 10(f)) at $T > T_N$ of Cr + 0.16 at.% Ga, and for the γ_L–T curve (figure 11(c)), both for $T > T_N$ and $T < T_N$, for Cr + 0.42 at.% Ga. Another problem is that, even for these cases, we could not measure γ very close to T_N, due to very high attenuation that is out of the reach of our equipment in the close proximity of T_N. Plots of $\log \gamma$, after subtracting the background attenuation, against $\log(|T/T_N - 1|)$ were found to be approximately straight lines in useful temperature regions both below and above T_N only for γ_{11} of Cr + 0.16 at.% Ga and for γ_L at $T > T_N$ for Cr + 0.42 at.% Ga. No useful linear regions on the log–log plots could be found for the other cases mentioned above. The T_N-values used in these plots were taken at the midpoints of the γ–T curves in figures 10(e) and 11(c). Small adjustments of T_N did not improve the fits. The best fits were for T_N obtained as explained above. The exponent of $|T_N/T - 1|$, determined from the straight-line plots, is given in table 5 for the cases for which it could be determined meaningfully. Both the Cr + 0.16 at.% Ga and Cr + 0.42 at.% Ga crystals show a transition from the P to the ISDW phase when cooled through T_N and should therefore give a divergence as $(T/T_N - 1)^{-1/2}$ for $T > T_N$ according to Sato and Maki's theory. From table 5, however, the measured exponent for $T > T_N$ is much smaller than $-\frac{1}{2}$. We do not know the reason for the discrepancy between theory and experiment, but the fact that our measurements could not be made close enough to T_N may play a role in this.

Magnetic anomalies in the elastic constants and thermal expansion of Cr alloys were recently studied theoretically by Katsnel'son and Trefilov [27]. They considered the effects of the disappearance of the antiferromagnetic SDW energy gap in the electron spectrum on the electron screening and phonon spectrum of the alloys, and showed that there is a negative SDW contribution to the thermal expansion coefficient at T_N. The theory furthermore predicts a softening in the elastic constants at T_N with a much larger softening in B than in the shear constants. Katsnel'son and Trefilov [27] found that the magnetic contributions to the thermal expansion and to the shear constants should vary as $(T_N - T)^{-1}$ if the density-of-states function in the paramagnetic phase is smooth near the Fermi level and as $(T_N - T)^{-5/4}$ if it has a van Hove singularity there. These power laws are valid [27] if the temperature is not too close to T_N. The present measurements on the elastic constants and thermal expansion of the Cr–Ga alloy single crystals allow for a test of Katsnel'son and Trefilov's theory. Only qualitative agreement was found with the theory. As predicted, the magnetic contribution to the thermal expansion of the Cr–Ga alloys is negative, while the bulk modulus shows a substantial softening with very slight or no softening below T_N for the shear constants. This qualitative agreement is also found for most other dilute Cr alloy systems. Quantitatively the theory was only tested up to now for Cr–Ir alloy single crystals [19] for which the experimental data are not fitted by the power laws $(T_N - T)^{-1}$ or $(T_N - T)^{-5/4}$. For the present Cr–Ga alloy single crystals neither ΔB or $\Delta\beta$ could be fitted successfully to any power law of the form $(T_N - T)^{-k}$. The theory fails quantitatively also in this case. The magnetic contributions to the shear mode elastic constants are too small to allow for a successful testing of the theory.

5. Summary and conclusions

The elastic constants, ultrasonic attenuation and thermal expansion of Cr–Ga alloy single crystals were studied for the first time. The spin-density wave has a very large softening effect on the longitudinal mode elastic constants and on the bulk modulus of these alloys near T_N while its effect on the shear mode elastic constants is nearly negligible. Volume strain terms in the magnetic free energy of these crystals therefore seem to dominate shear terms, making the Cr–Ga system very suitable for testing the predictions of thermodynamic models for the magnetoelasticity of dilute Cr alloys. The model correctly predicts the temperature dependence of the magnetic contributions to the bulk modulus and of the magnetovolume in the incommensurate spin-density-wave state of the alloys. The volume derivative of the Néel temperature calculated from the magnetoelastic measurements on the Cr–Ga alloy single crystals, using the thermodynamic model, compares very well with the results of direct high-pressure measurements. This is however not the case for the volume derivative of the incommensurate–commensurate spin-density-wave magnetic phase transition temperature. The short-range magnetic order and spin fluctuations in Cr–Ga alloys above the Néel temperature (T_N) were found to be less volume dependent than the spin-density wave below T_N, in contrast to what is found for most other dilute Cr alloy systems. Theoretical predictions of the temperature divergence of the ultrasonic attenuation coefficient near T_N are not fulfilled by the measurements on the Cr–Ga alloys. This is also the case for the predictions of recent microscopic theories for the magnetic contributions to the thermal expansion.

References

[1] Fawcett E, Alberts H L, Galkin Yu V, Noakes D R and Yakhmi J V 1994 *Rev. Mod. Phys.* **66** 25
[2] Alberts H L and Smit P 1994 *J. Phys.: Condens. Matter* **6** 3661
[3] Baran A, Alberts H L, Strydom A M and du Plessis P de V 1992 *Phys. Rev.* B **45** 10 473
[4] Alberts H L 1989 *J. Phys.: Condens. Matter* **1** 4993
[5] Alberts H L 1994 *J. Appl. Phys.* **75** 5665
[6] Alberts H L and Lourens J A J 1984 *Phys. Rev.* B **29** 5279
[7] Alberts H L and Lourens J A J 1985 *J. Phys. F: Met. Phys.* **15** 2511
[8] Anderson R A, Alberts H L and Smit P 1993 *J. Phys.: Condens. Matter* **5** 1733
[9] Bohlman M and Alberts H L 1970 *J. Phys. E: Sci. Instrum.* **3** 779
[10] Papadakis E P 1976 *Physical Acoustics* vol 12, ed W P Mason and R N Thurston (New York: Academic)
[11] Nye J F 1957 *Physical Properties of Crystals* (Oxford: Clarendon)
[12] Roberts R B, White G K and Fawcett E 1983 *Physica* B **119** 63
[13] Alberts H L and Lourens J A J 1985 *J. Phys. F: Met. Phys.* **15** L49
[14] Fernandez-Baca J A, Fawcett E, Alberts H L, Galkin Yu V and Endoh Y 1997 *J. Appl. Phys.* **81** 3877
[15] Truel R, Elbaum C and Chick B B 1969 *Ultrasonic Methods in Solid State Physics* (New York: Academic)
[16] Kittinger E 1977 *Ultrasonics* **15** 30
[17] Alberts H L 1990 *J. Phys.: Condens. Matter* **2** 9707
[18] de Camaro P C, Fawcett E and Perez J M 1990 *J. Appl. Phys.* **67** 5265
[19] Martinova J, Alberts H L and Smit P 1997 *J. Phys.: Condens. Matter* **9** 3461
[20] Cankurtaran M, Saunders G A, Wang Q, Ford P J and Alberts H L 1992 *Phys. Rev.* B **46** 14 370
[21] Fawcett E and Alberts H L 1992 *J. Phys.: Condens. Matter* **4** 613
[22] Fawcett E and Alberts H L 1990 *J. Phys.: Condens. Matter* **2** 6251
[23] Alberts H L and Lourens J A J 1992 *J. Phys.: Condens. Matter* **4** 3835
[24] Bloch D and Pavlovic H 1969 *Advances in High Pressure Research* ed R S Bradley (New York: Academic)
[25] Prinsloo A R E, Alberts H L and Smit P 1997 *Physica* B **273** 419
[26] Sato H and Maki K 1973 *Int. J. Magn.* **4** 163
[27] Katsnel'son M I and Trefilov A V 1994 *Phys. Met. Metallogr.* **77** 362